IEEE Access
Multidisciplinary | Rapid Review | Open Access Journal

Received February 7, 2018, accepted March 22, 2018, date of publication April 2, 2018, date of current version April 23, 2018.

Digital Object Identifier 10.1109/ACCESS.2018.2821766

Performance Analysis for Focused Beamformers in Passive Underwater Acoustic Localization

JUN LI[1,2], (Student Member, IEEE), QIU-HUA LIN[1], (Member, IEEE), KAI WANG[3], AND CHUN-YU KANG[2]

[1]School of Information and Communication Engineering, Faculty of Electronic Information and Electrical Engineering, Dalian University of Technology, Dalian, Liaoning 116024, China
[2]Department of Underwater Weaponry and Chemical Defense, Dalian Naval Academy, Dalian, Liaoning 116018, China
[3]Department of Computer Science and Technology, Dalian Neusoft Institute of Information, Dalian, Liaoning 116023, China

Corresponding author: Jun Li (lijunwk@163.com)

This work was supported by the National Natural Science Foundation of China under Grant 61471378.

ABSTRACT Focused beamformers are widely used in passive underwater acoustic localization. Many pseudo-peaks (spurious peaks not corresponding to a real source) are produced by focused beamformers, impacting the performance and reliability of related algorithms. After describing both the received signal model of near-field sources with a uniform line array, and the basic principle of passive localization based on focused beamformers, we define pseudo-peaks in the focused beamformer's spectra and give the procedure to quantify these pseudo-peaks. The performance of conventional focused beamformers (C-FBs) and minimum variance distortionless response focused beamformers (MVDR-FBs) are studied, focusing on the number of pseudo-peaks in passive underwater acoustic localization. After establishing a simulation model based on an underwater acoustic environment, the algorithms are compared in terms of signal-to-noise ratio, frequency, distance of the source signal, and detection threshold. In all cases, the MVDR-FB method shows superior performance to the C-FB method in minimizing the number of pseudo-peaks. Finally, a method of selecting the detection threshold based on the convergence of pseudo-peak number is proposed.

INDEX TERMS Focused beamformer, performance analysis, sensor arrays, underwater acoustics.

I. INTRODUCTION

Passive localization technology is widely used in sonar. Its advantage is that, without transmitting, the delivery platform retains good concealment. Most existing sensor array signal processing techniques for passive localization assume that the signal sources are relatively far from the array of sensors, so the waves impinging on the array are far-field and thus appear as plane waves [1], [2]. Therefore, those methods can only estimate the source's direction and cannot estimate the source's distance.

In the near-field environment, the plane-wave approximation of the spherical wave-fronts is no longer valid. The spherical wave-fronts model is more accurate [3]–[5]. Recently, many methods have been proposed to estimate the target's direction and distance in the near-field, or mixed near-field and far-field, environment [2]–[15]. The conventional focused beamformer (C-FB) method and minimum variance distortionless response focused beamformer (MVDR-FB) method are two such methods. Hui *et al.* [6] used a C-FB to measure the distribution image (underwater image) of a ship's noise sources. Shi *et al.* [7] and Shi and Yang [8] proposed two new methods of coherent broadband MVDR-FBs based on vector sensor array processing. Kumar and Hegde [9] used MVDR-FBs to address the method of near-field source localization using a spherical microphone array. Somasundaram *et al.* [10] proposed a low-complexity, quickly-converging, robust adaptive beamformer method for large arrays in snapshot deficient scenarios. Salvati *et al.* [11] proposed a weighted MVDR algorithm based on a machine learning component for near-field sound localization in a reverberant environment. For the mixed far-field and near-field sources localization problem, Liang and Liu [4] presented a fourth-order cumulants-based Toeplitz matrix reconstruction method. Liu and Sun [12] and [13] presented a covariance difference algorithm and a novel classification localization algorithm. Thus, both the C-FB and MVDR-FB methods have proven their usefulness in a wide variety of applications.

However, many pseudo-peaks (spurious peaks which do not correspond to an actual source) are produced by focused

beamformers in passive localization, and those pseudo-peaks may seriously impact the performance of the algorithms when there are multiple sound sources. In the spatial spectrum of sonar detection, the number of pseudo-peaks is seriously affected by the detection threshold. When the detection threshold is small, many pseudo-peaks appear in the spatial spectrum, and the target energy spectrum is submerged in a number of spurious peaks, forming a 'sky star' detection pattern. It is difficult to determine which targets are real and which are spurious. When the detection threshold is large, the number of pseudo-peaks is greatly reduced, but the true target energy spectrum may be filtered out, resulting in a false negative. Therefore, the choice of pseudo-peak detection threshold is very important.

There are few papers about the pseudo-peaks made by focused beamformers [14], or about the pseudo-peak detection threshold setting, in passive underwater acoustic localization. In this paper, we provide criteria for identifying pseudo-peaks in the focused beamformer's spectra and show how to derive the quantity of pseudo-peaks. After establishing a simulation model based on a typical underwater acoustic environment, simulation results are presented to compare the performance of the C-FB and MVDR-FB, and the influence of the detection threshold on the number of pseudo-peaks, in a variety of different conditions. The conditions varied are signal to noise ratio (SNR), the sound source's frequency, the distance between sound source and hydrophones, and the detection threshold value. Finally, we propose a method to set the detection threshold according to the convergence of the number of pseudo-peaks.

The rest of this paper is organized as follows. The signal model for the near-field is introduced in Section 2. The two types of focused beamformer, the pseudo-peak definition, and the pseudo-peak quantity survey are developed in Section 3. Simulation results are presented in Section 4. Conclusions are drawn in Section 5.

II. NEAR-FIELD SIGNAL MODEL

Following Cirpan and Cekli [1], we consider the near-field underwater acoustic environment with a uniform linear array in which narrowband signals from d sources are received by an M element hydrophone. Let the first hydrophone be the phase reference point with index '1' as shown in Fig. 1.

Assuming the spacing of sensors is Δ, the narrowband output signal of the sensor m is given by

$$x_m(t) = \sum_{i=1}^{d} s_i(t - \tau_{im}) + n_m(t), \tag{1}$$

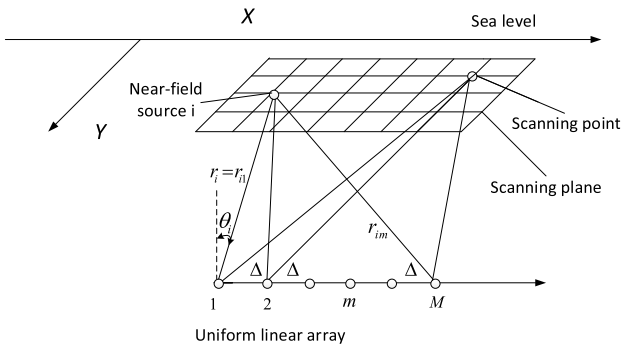

FIGURE 1. The principle of focused beamformer passive localization with a uniform linear array.

where $s_i(t)$ denotes the complex envelope of the source signal i, $n_m(t)$ is an additive complex Gaussian noise, and τ_{im} is the delay of the source signal i relative to the reference sensor. The analytic signal of (1) is:

$$x_m(t) = \sum_{i=1}^{d} s_i(t) e^{-j\phi_{im}} + n_m(t), \tag{2}$$

where ϕ_{im} is the phase difference of the signal i collected at sensor m with respect to the signal i collected at reference sensor '1'. Due to our narrowband assumption, the phase difference is given by

$$\phi_{im} = \frac{2\pi}{\lambda} (r_{im} - r_i), \tag{3}$$

where λ is the wavelength of the source signal. The distance r_{im} between the source i and the sensor m equals

$$\begin{aligned} r_{im} &= \sqrt{r_i^2 + (m-1)^2 \Delta^2 - 2 r_i (m-1) \Delta \sin\theta_i} \\ &= r_i \sqrt{1 + \frac{(m-1)^2 \Delta^2}{r_i^2} - \frac{2(m-1)\Delta}{r_i} \sin\theta_i}, \end{aligned} \tag{4}$$

Substituting (4) and (3) into (2), we obtain (5), as shown at the bottom of this page.

For a collection of M observed sensor outputs $\boldsymbol{X} = [x_1(t), \cdots, x_M(t)]^{\mathrm{T}}$, and the matrix formulation of (5) is obtained as follows:

$$\boldsymbol{X} = \boldsymbol{A}(\theta, r) \cdot \boldsymbol{S} + \boldsymbol{N}, \tag{6}$$

where $\boldsymbol{N} = [n_1(t), \cdots, n_M(t)]^{\mathrm{T}}$ is Gaussian white noise. $\boldsymbol{S} = [s_1(t), \cdots, s_d(t)]^{\mathrm{T}}$ is the collection of d impinging signals written as a column vector, and $\boldsymbol{A}(\theta, r) = [a(\theta_1, r_1), \cdots, a(\theta_d, r_d)]$ is the array steering matrix in the near-field case which is a function of an unknown set of parameters $\{\theta, r\} = \{(\theta_1, r_1), \cdots, (\theta_d, r_d)\}$.

$$x_m(t) = \sum_{i=1}^{d} \left(s_i(t) \exp\left(-j \frac{2\pi \left(\sqrt{r_i^2 + (m-1)^2 \Delta^2 - 2 r_i (m-1) \Delta \sin\theta_i} - r_i \right)}{\lambda} \right) + n_m(t) \right), \tag{5}$$

III. FOCUSED BEAMFORMER AND ITS PSEUDO-PEAK

A. CONVENTIONAL FOCUSED BEAMFORMER

Following the work of Hui *et al.* [6] and Shi *et al.* [7], the principle of focused beamformer passive underwater acoustic localization is shown in Fig. 1. Using each array element's source radius of curvature, the delay difference is compensated based on the spherical wave-fronts model. The delay difference is a two-dimensional function determined by the source's direction and distance. By scanning the different focal points of the scanning plane, the sound intensity diagram of the scanning plane is obtained. When the scanning point coincides with the target position, the output of the focused beam will peak. Therefore, the target's direction and distance information can both be obtained via a focused beamformer.

According to the model of the uniform linear array, the output of a C-FB is obtained as follows:

$$y(t) = \sum_{i=1}^{M} x_i \left(t + \frac{r_{1i} - r_1}{c} \right), \tag{7}$$

where c is the underwater sound velocity, r_1 is the distance of a scanning point to the reference array element, and r_{1i} is the distance of scanning point (θ_1, r_1) to the array element i. According to (4), $r_{1i} = \sqrt{r_1^2 - 2(i-1)r_1\Delta\sin\theta_1 + (i-1)^2\Delta^2}$, where θ_1 is the direction of the scanning point to the reference array element. The output is obtained as follows:

$$y(t) = \sum_{i=1}^{M} x_{im}(t) \exp\left(j2\pi \frac{r_{1i} - r_1}{\lambda} \right) = \boldsymbol{W}^H \boldsymbol{X}, \tag{8}$$

where the weight vector $\boldsymbol{W}$ is

$$\boldsymbol{W} = [1, e^{j2\pi \frac{r_{12} - r_1}{\lambda}}, \cdots, e^{j2\pi \frac{r_{1M} - r_1}{\lambda}}]^T, \tag{9}$$

and the output spatial spectrum is

$$\begin{aligned} P_{C-FB}(\theta, r) &= E\{|y(t)|^2\} = E\left\{ \left| \boldsymbol{W}^H X \right|^2 \right\} \\ &= \boldsymbol{W}^H E\left\{ \boldsymbol{X}(t)\boldsymbol{X}^H(t) \right\} \boldsymbol{W} = \boldsymbol{W}^H \boldsymbol{R}_{XX} \boldsymbol{W}, \end{aligned} \tag{10}$$

where $\boldsymbol{R}_{XX} = E\left\{ \boldsymbol{X}(t)\boldsymbol{X}^{\mathrm{H}}(t) \right\}$ is the covariance matrix of the uniform linear array output.

When the scanning point coincides with the target position, the output of $P_{C-FB}(\theta, r)$ will peak and we can obtain the maximum output in the spatial spectrum.

B. MVDR FOCUSED BEAMFORMER

The MVDR-FB is an adaptive beamformer method [7]–[11]. It can suppress noise in nonsource directions, and ensure that the energy of the signal in the source direction remains constant. Bell *et al.* [16] and Capon [17] proposed the optimization criterion for determining direction, and this section extends this optimization criterion to directional and distance spaces.

We assume that there is a desired signal $d(t)$ (its spatial position is (θ_d, r_d)) and J interference signals $z_j(t), j = 1, \cdots, J$ (their spatial positions are (θ_{zj}, r_{zj})) in the space. Then the received signals of each element can be expressed as:

$$\begin{aligned} \boldsymbol{X}(t) &= \boldsymbol{A}\boldsymbol{S}(t) + \boldsymbol{N}(t) \\ &= \boldsymbol{a}(\theta_d, r_d) d(t) + \sum_{j=1}^{J} \boldsymbol{a}(\theta_{zj}, r_{zj}) z_j(t) + \boldsymbol{N}(t), \end{aligned} \tag{11}$$

Substituting (11) into (10) and simplifying, we obtain the output spatial spectrum:

$$\begin{aligned} &P(\theta_d, r_d) \\ &= E\left\{ |d(t)|^2 \right\} \left| \boldsymbol{W}^H \boldsymbol{a}(\theta_d, r_d) \right|^2 \\ &\quad + \sum_{j=1}^{J} E\left\{ \left| z_j(t) \right|^2 \right\} \left| \boldsymbol{W}^H \boldsymbol{a}(\theta_{zj}, r_{zj}) \right|^2 + \sigma_n^2 \left\| \boldsymbol{W} \right\|^2, \end{aligned} \tag{12}$$

The expression in (12) is divided into three parts: the output energy of the desired signal $E\left\{ |d(t)|^2 \right\} \left| \boldsymbol{W}^H \boldsymbol{a}(\theta_d, r_d) \right|^2$, the output energy of interference signals $\sum_{j=1}^{J} E\left\{ \left| z_j(t) \right|^2 \right\} \left| \boldsymbol{W}^H \boldsymbol{a}(\theta_{zj}, r_{zj}) \right|^2$, and the output energy of noise $\sigma_n^2 \left\| \boldsymbol{W} \right\|^2$.

In order to ensure the correct reception of the desired signal from the position (θ_d, r_d) and completely suppress the J interference in other positions, we obtain the constraint conditions on the weight vector from (12):

$$\boldsymbol{W}^{\mathrm{H}} \boldsymbol{a}(\theta_d, r_d) = 1, \tag{13}$$

$$\boldsymbol{W}^{\mathrm{H}} \boldsymbol{a}(\theta_{zj}, r_{zj}) = 0, \tag{14}$$

Under these two constraints, (12) reduces to:

$$P(\theta_d, r_d) = \boldsymbol{W}^{\mathrm{H}} \boldsymbol{R}_{XX} \boldsymbol{W} = E\left\{ |d(t)|^2 \right\} + \sigma_n^2 \left\| \boldsymbol{W} \right\|^2, \tag{15}$$

According to (13) and (14), although the selected weight vector can maximum the desired signal output energy, and reduce the interference output to zero, it may also make the noise output energy more prominent. Therefore, the suppression of interference and noise should be considered together. In (15), $E\left\{ |d(t)|^2 \right\}$ is a constant, and $\sigma_n^2 \left\| \boldsymbol{W} \right\|^2$ is the energy of noise. If we want to minimize the noise output energy, we have to minimum the $P(\theta_d, r_d)$. Therefore, the optimal weight vector of MVDR-FB can be described by the following optimization problem:

$$\begin{aligned} &\min_{\boldsymbol{W}} \boldsymbol{W}^{\mathrm{H}} \boldsymbol{R}_{XX} \boldsymbol{W} \\ &s.t.\ \boldsymbol{W}^{\mathrm{H}} \boldsymbol{a}(\theta_d, r_d) = 1, \end{aligned} \tag{16}$$

where $\boldsymbol{W} = [w_1, w_2, \cdots w_M]^{\mathrm{T}}$ is a weight vector, $\boldsymbol{a}(\theta_d, r_d)$ is the direction and distance vector of the uniform linear array, and $\boldsymbol{R}$ is the covariance matrix of the uniform linear array output. The Lagrange method is usually used to solve

the above constrained optimization problems [16], [17]. The optimal weight vector is obtained as follows:

$$\boldsymbol{W}_{opt} = \frac{\boldsymbol{R}^{-1}\boldsymbol{A}(\theta, r)}{\boldsymbol{A}(\theta, r)^{\mathrm{H}}\boldsymbol{R}^{-1}\boldsymbol{A}(\theta, r)}, \tag{17}$$

where (θ, r) is the scanning point. The spatial spectrum of MVDR-FB equals:

$$\boldsymbol{P}_{MVDR-FB}(\theta, r) = \boldsymbol{W}_{opt}^{\mathrm{H}}\boldsymbol{R}\boldsymbol{W}_{opt} = \frac{1}{\boldsymbol{A}(\theta, r)^{\mathrm{H}}\boldsymbol{R}^{-1}\boldsymbol{A}(\theta, r)}, \tag{18}$$

From (18), the output spatial spectrum is a two-dimensional function determined by the source's direction and distance. When the scanning point (θ, r) coincides with the true target position (θ_s, r_s), the output of $\boldsymbol{P}_{MVDR-FB}(\theta, r)$ will reach a maximum value, and the source location can be estimated from the peak of the spatial spectrum.

C. PSEUDO-PEAKS AND QUANTITY SURVEY

Note that the output matrix $\boldsymbol{P}$ is a normalized spatial spectrum, whose elements $P(\theta_m, r_n)$ are functions of direction θ and range r. For convenience, we assume that the target is located in the range of the scanning space and not at the edge of the spatial spectrum matrix $\boldsymbol{P}$. Thus, in the process of calculating the pseudo-peak, the edge elements of $\boldsymbol{P}$ are excluded, and we can only find pseudo-peaks in $\tilde{\boldsymbol{P}}$, which is composed of $\boldsymbol{P}$ without $\boldsymbol{P}$'s edge elements. $\tilde{\boldsymbol{P}}$ has the following form:

$$\tilde{\boldsymbol{P}} = \begin{bmatrix} P(\theta_2, r_2) & P(\theta_2, r_3) & \cdots & P(\theta_2, r_{N-1}) \\ P(\theta_3, r_2) & P(\theta_3, r_3) & \cdots & P(\theta_3, r_{N-1}) \\ \vdots & \vdots & \ddots & \vdots \\ P(\theta_{M-1}, r_2) & P(\theta_{M-1}, r_3) & \cdots & P(\theta_{M-1}, r_{N-1}) \end{bmatrix}, \tag{19}$$

In addition, we identify $P(\theta_m, r_{n-1})$, $P(\theta_m, r_{n+1})$, $P(\theta_{m+1}, r_n)$, and $P(\theta_{m-1}, r_n)$ as the adjacent elements of $P(\theta_m, r_n)$. The element $P(\theta_m, r_n)$ and its adjacent elements are shown in Fig. 2. Each of $\tilde{\boldsymbol{P}}$'s elements has four adjacent elements in $\boldsymbol{P}$. To handle elements with small values, we assume that there is a detection threshold γ. If $P(\theta_m, r_n) < \gamma$, the element $P(\theta_m, r_n)$ is not a pseudo-peak.

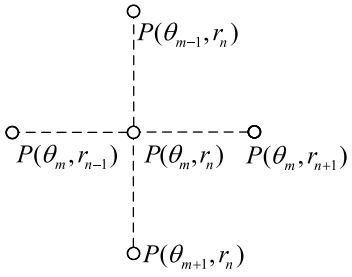

FIGURE 2. One element and its adjacent elements.

Based on the aforementioned analyses, the protocol for determining the pseudo-peaks in $\boldsymbol{P}$ is proposed as follows. The necessary conditions for the element $P(\theta_m, r_n)$ to be a pseudo-peak are:

1. The sound sources (target) are not at (θ_m, r_n).

If the sound sources are at (θ_m, r_n), $P(\theta_m, r_n)$ will be a main peak. The pseudo-peaks are those peaks that do not contain targets.

2. $P(\theta_m, r_n) \in \tilde{\boldsymbol{P}}$.

In this condition, we need not consider the edge elements of $\boldsymbol{P}$, and the pseudo-peaks can be found easily.

3. $P(\theta_m, r_n) \geq \gamma$.

The value of γ can affect the number of pseudo-peaks greatly. If γ varies from a small value to a large value, the estimated quantity of pseudo-peaks will decrease. Through estimating the number of pseudo-peaks in terms of γ, we can find the main distribution range of the pseudo-peaks' amplitudes.

4. The element $P(\theta_m, r_n)$ must meet one of the following conditions:

a. $P(\theta_m, r_n)$ is greater than its all adjacent elements:

$$\begin{aligned} &P(\theta_m, r_n) > P(\theta_m, r_{n-1}), P(\theta_m, r_n) > P(\theta_m, r_{n+1}) \\ &P(\theta_m, r_n) > P(\theta_{m-1}, r_n), P(\theta_m, r_n) > P(\theta_{m+1}, r_n), \end{aligned} \tag{20}$$

b. $\boldsymbol{Q}$ is a continuous area with many elements in $\boldsymbol{P}$, and each element of $\boldsymbol{Q}$ is equal to a fixed value α_Q, where α_Q is greater than all $\boldsymbol{Q}$'s adjacent elements. An example of such a continuous area $\boldsymbol{Q}$ and its adjacent elements is shown in Fig. 3. From Fig. 3, we can see that the points 1–12 are $\boldsymbol{Q}$'s elements and the points 13–25 are $\boldsymbol{Q}$'s adjacent elements.

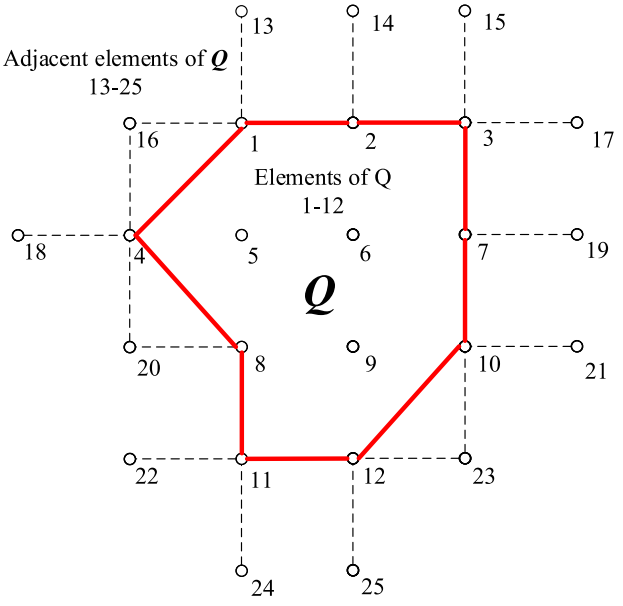

FIGURE 3. A continuous area Q with many elements, and its adjacent elements.

Some representative examples of pseudo-peaks in a part of the spatial spectrum are shown in Fig. 4. We assume that

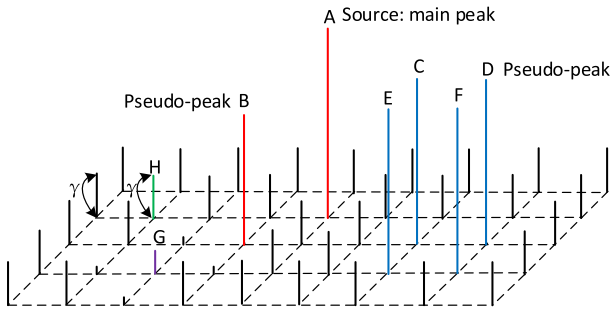

FIGURE 4. Some representative examples of pseudo-peaks.

the sound source (target) is only at point A and the detection threshold γ is equal to the value of point H, so the peak at point A is the main peak. In addition, the peak at point B is a typical pseudo-peak, because it meets conditions 1-3 as well as 4a. However, the peak at point G is not a pseudo-peak, because G's value is less than the detection threshold γ (thus, it does not meet condition 3). We conclude that the peaks at points C, D, E, and F are only one pseudo-peak because the values at C, D, E, and F are equal. Following the above discussion, we can easily evaluate the quantity of pseudo-peaks in a normalized output spatial spectrum, and also study the relationship between the detection threshold and the quantity of pseudo-peaks.

IV. SIMULATIONS

Four simulations were conducted to evaluate the performance of the proposed algorithms. We considered a 32-element uniform linear array with element spacing $d = 1$m, where the sound source was a single-frequency signal. In addition, the scan distance range was 1–3000 m with a 1 m step length and the scan direction range was $(-60°, 60°)$ with a $1°$ step length. The number of snapshots was $K = 2048$ and the sampling frequency was $fs = 125$ kHz. We assumed that the received signals were polluted by additive white Gaussian noise and the speed of sound was $c = 1500$m/s. The performances of the proposed algorithms were measured by the estimated pseudo-peaks' quantity over 100 independent Monte Carlo runs.

A. SNR IMPACT

In this simulation, the C-FB and MVDR-FB algorithms were used to analyze a near-field source which was located at $(\theta = 20°,\ r = 2500\ m)$. The frequency of the source was set to 20 kHz. The spatial spectra achieved by C-FB and MVDR-FB with two different SNRs (0 dB, 10 dB) are shown in Fig. 5 and Fig. 6.

From Fig. 5 and Fig. 6, we can see that when the SNR decreases, more pseudo-peaks in the spatial spectra are obtained by both C-FB and MVDR-FB. The pseudo-peaks represent numerous false targets which may affect the accuracy of localization.

As the SNR in the marine environment is generally distributed between -20 dB and 20 dB, we studied the effect of

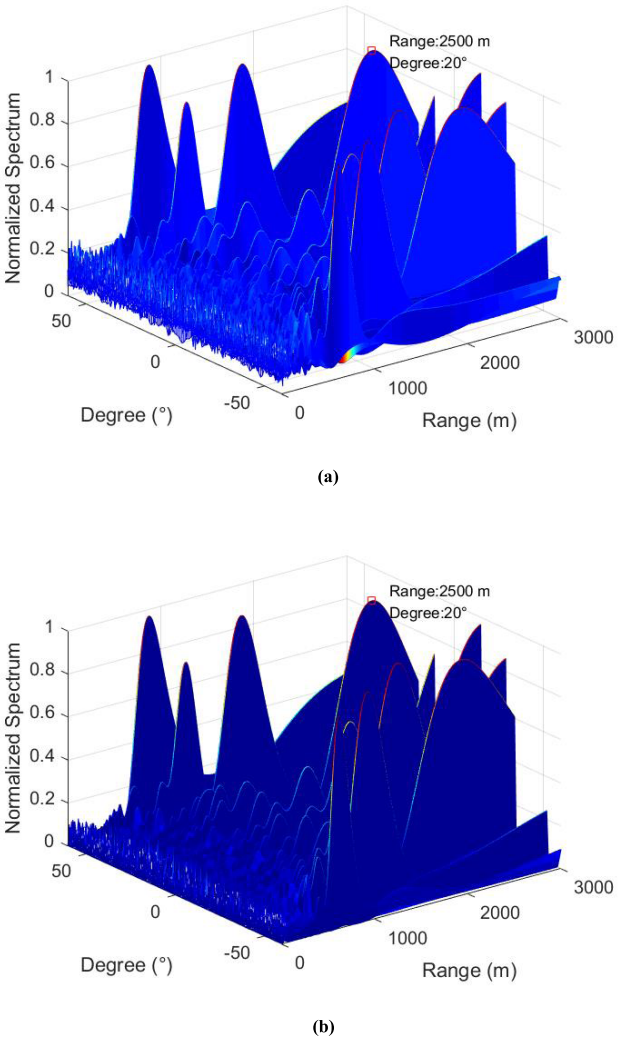

FIGURE 5. Localization results of C-FB with different SNRs. (a) SNR = 0 dB. (b) SNR = 10 dB.

the SNR in this interval on the performance of the algorithms. When SNR varies from -20 to 20 dB and the detection threshold γ is fixed at 0.2 or 0.4, the number of pseudo-peaks produced by C-FB and MVDR-FB are shown in Fig. 7. This figure shows that the noise immunity of MVDR-FB outperforms that of C-FB. In addition, the direction and distance estimation accuracy of MVDR-FB also surpass the conventional method. When the SNR increases, the number of pseudo-peaks in spatial spectra obtained by MVDR-FB decreases more quickly than C-FB, and the number of pseudo-peaks converges.

The pseudo-peaks produced by C-FB will always exist. When the threshold value γ was set equal to 0.2 or 0.4, the pseudo-peaks' quantity converged to 28 or 8, respectively. However, the pseudo-peaks produced by MVDR-FB disappeared when the SNR increased to about 10 dB. Thus, for modestly high SNR, the MVDR-FB method eliminates the problem of pseudo-peaks entirely, unlike C-FB.

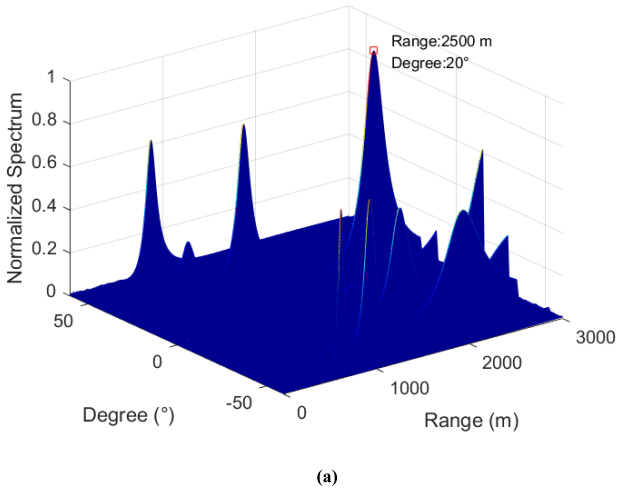

(a)

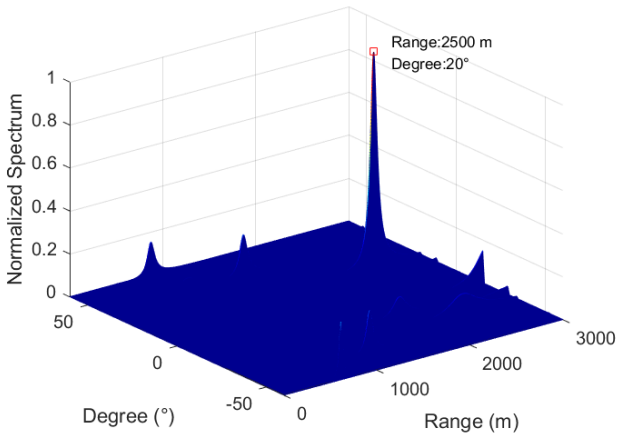

(b)

FIGURE 6. Localization results of MVDR-FB with different SNRs. (a) SNR = 0 dB. (b) SNR = 10 dB.

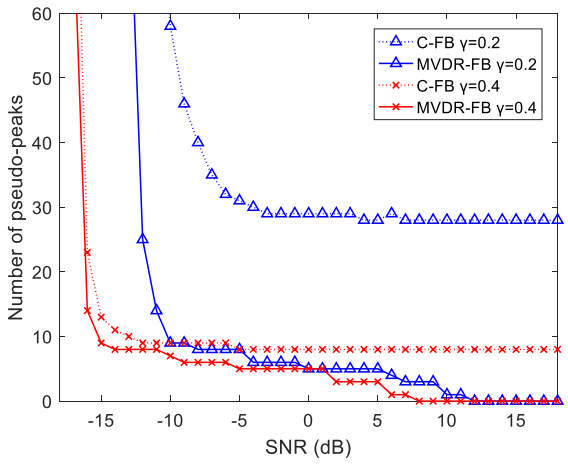

FIGURE 7. The number of pseudo-peaks in terms of SNR.

B. FREQUENCY IMPACT

In this simulation, the influence of the sound source's frequency on the algorithm's performance was studied.

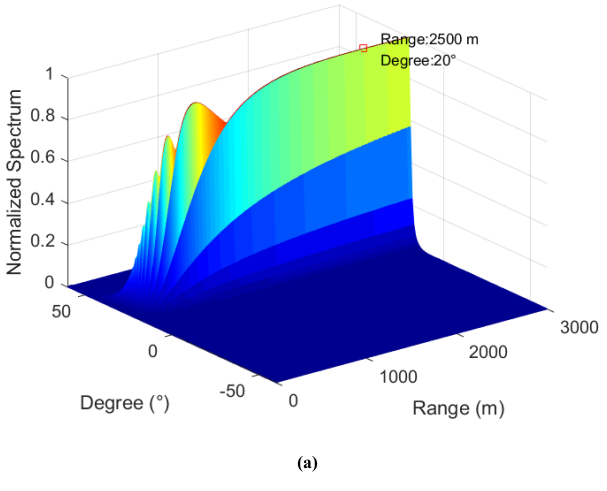

(a)

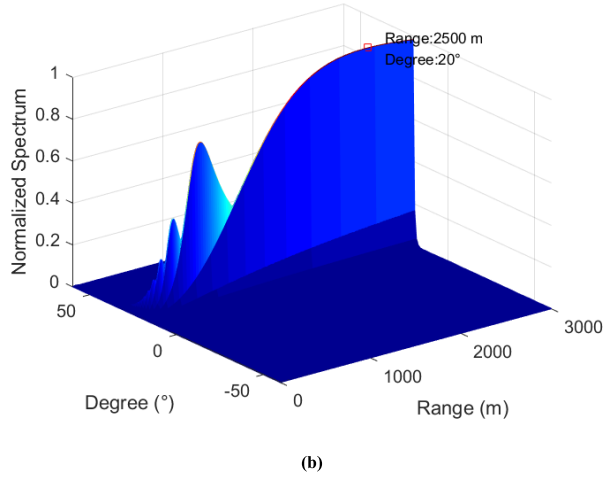

(b)

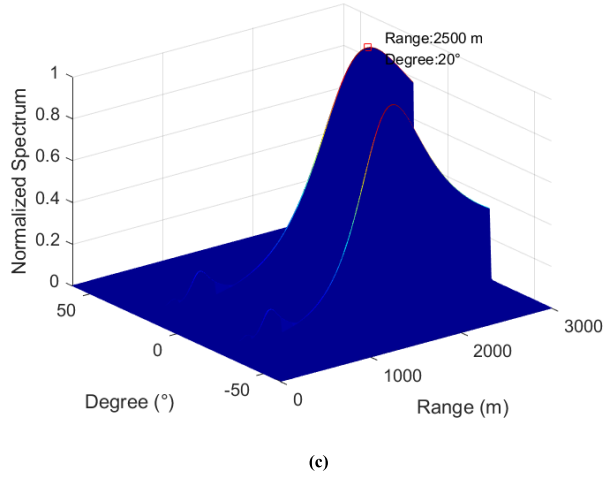

(c)

FIGURE 8. Localization results of MVDR with different frequencies. (a) frequency = 0.2 kHz. (b) frequency = 0.5 kHz. (c) frequency = 2 kHz.

The SNR was set equal to 5 dB and other conditions were the same as case 1. The spatial spectra achieved by MVDR-FB with three different frequencies (0.2 kHz, 0.5 kHz, and 2 kHz) are shown in Fig. 8.

From Fig. 8, we can see that when the frequency of the sound source was lower than 0.5 kHz, MVDR-FB could only obtain the target's direction accurately, and could not estimate the distance accurately. However, as the frequency increased, the spatial spectra gradually became sharper. When the frequency was above 2 kHz, the target's direction and distance could be estimated accurately by MVDR-FB.

The working frequencies of most sonars are in the range of 1-50 kHz, so it is more practical to study the performance of the algorithm in that frequency band. When the frequency was varied from 1 to 50 kHz and the SNR was set equal to 0 dB, the number of pseudo-peaks produced by C-FB and MVDR-FB are shown in Fig. 9 and Fig. 10, respectively. The detection threshold γ was fixed at 0.1, 0.12, 0.15, and 0.2 for C-FB, and at 0.012, 0.015, 0.017, and 0.05 for MVDR-FB.

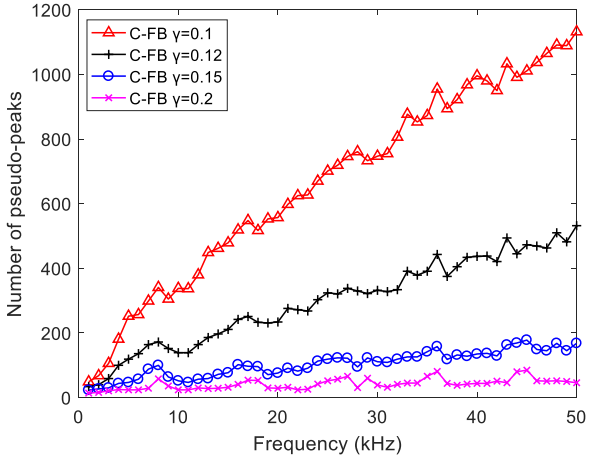

FIGURE 9. The number of pseudo-peaks with C-FB in terms of frequency.

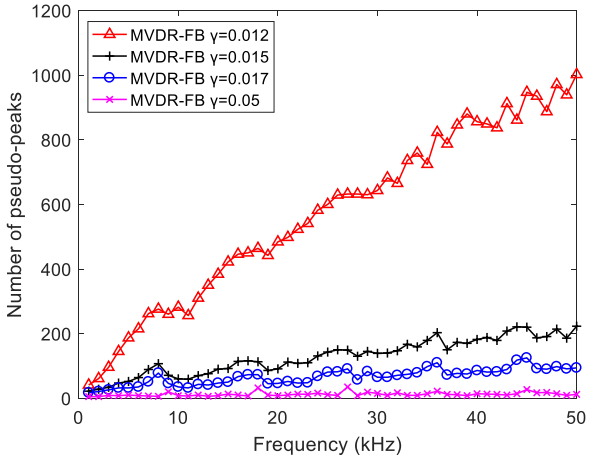

FIGURE 10. The number of pseudo-peaks with MVDR-FB in terms of frequency.

From Fig. 9 and Fig. 10, it can be seen that the number of pseudo-peaks increased as the frequency increased. However, this does not mean that the performance of the methods will drop as the frequency increases. The spectral peaks (including the main peak and pseudo-peaks) became sharper as the frequency increased, so the precision of estimation will be improved. Additionally, the amplitude of most pseudo-peaks was low, so they will have little effect on the estimation performance. In the spatial spectra achieved by C-FB, most of the pseudo-peaks' amplitudes were between 0.1 and 0.15. By comparison, in MVDR-FB's spatial spectra, most of the pseudo-peaks' amplitudes were only between 0.012 and 0.015. The performance of MVDR-FB was thus much higher than that of C-FB.

C. DISTANCE IMPACT

In this simulation, the influence of the sound source's distance on the algorithm's performance was studied. The SNR and frequency were set at 5 dB and 20 kHz respectively, and the other conditions were the same as case 1. The spatial spectra achieved by MVDR-FB with two different distances (200 m and 1000 m) are shown in Fig. 11.

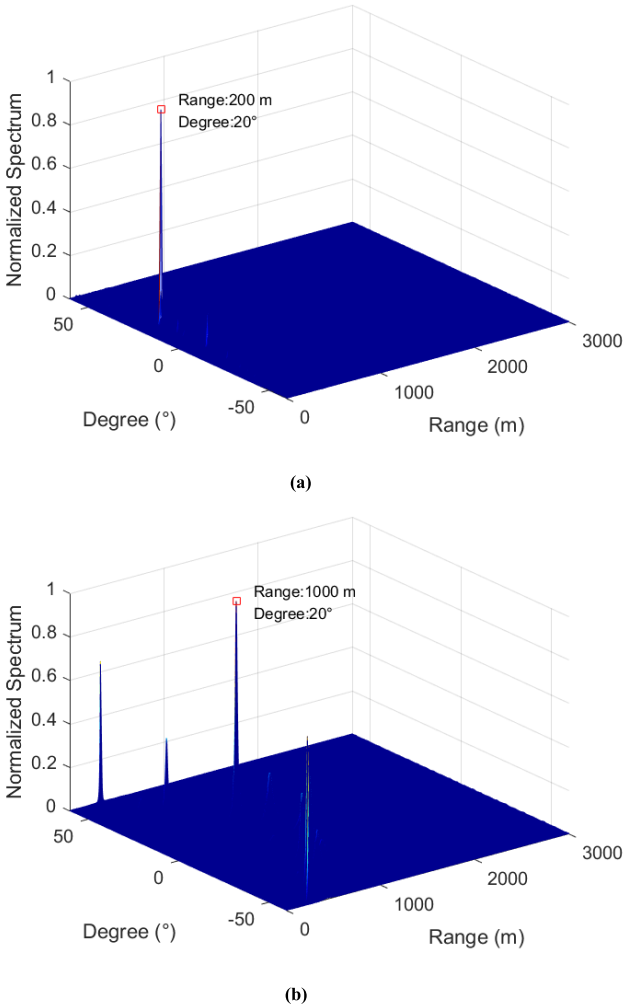

FIGURE 11. Localization results of MVDR-FB with different distances. (a) distance = 200 m. (b) distance = 1000 m.

From Fig. 11, we can see that when the distance of the sound source was shorter than 200 m, there were few pseudo-peaks in the spatial spectrum and the target's location can be

obtained accurately by MVDR-FB. As the distance increased, more pseudo-peaks in the spatial spectra were obtained by MVDR-FB.

When the distances varied from 50 to 2950 m and the SNR was set equal to 0 dB, the number of pseudo-peaks produced by C-FB and MVDR-FB are shown in Fig. 12 and Fig. 13, respectively. The detection threshold γ was fixed at 0.2, 0.3, and 0.4 for C-FB, and at 0.1, 0.2, and 0.4 for MVDR-FB.

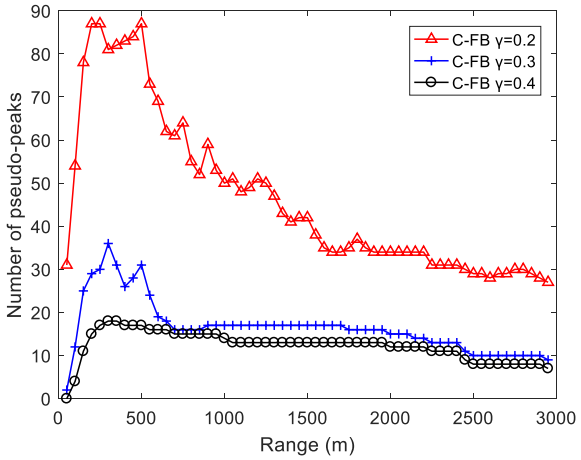

FIGURE 12. The number of pseudo-peaks with C-FB in terms of range.

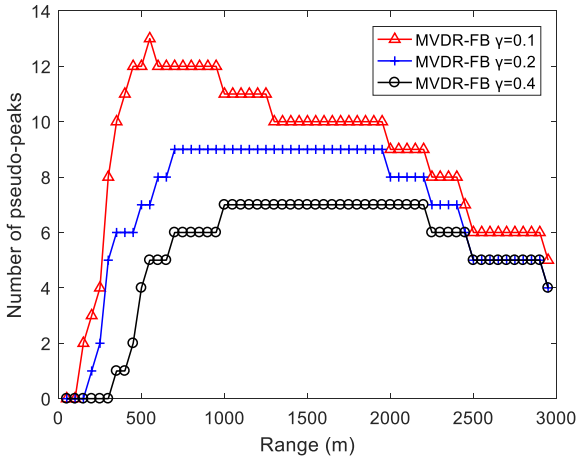

FIGURE 13. The number of pseudo-peaks with MVDR-FB in terms of range.

From Fig. 12 and Fig. 13, when the distances increased, the number of pseudo-peaks increased initially and then decreased. In the spatial spectra achieved by C-FB, most of the pseudo-peaks' amplitudes were between 0.2 and 0.3. By comparison, in MVDR-FB's spatial spectra, most of the pseudo-peaks' amplitudes were between 0.1 and 0.4. The number of pseudo-peaks obtained by MVDR-FB was less than C-FB.

D. THE DETECTION THRESHOLD IMPACT

In this simulation, the relationship between the number of pseudo-peaks and the detection threshold γ was studied. The SNRs were set at -10 dB and 0 dB, and the other conditions were the same as case 1. When the detection threshold γ varied from 0 to 1, the number of pseudo-peaks produced by the C-FB and MVDR-FB methods are shown in Fig. 14.

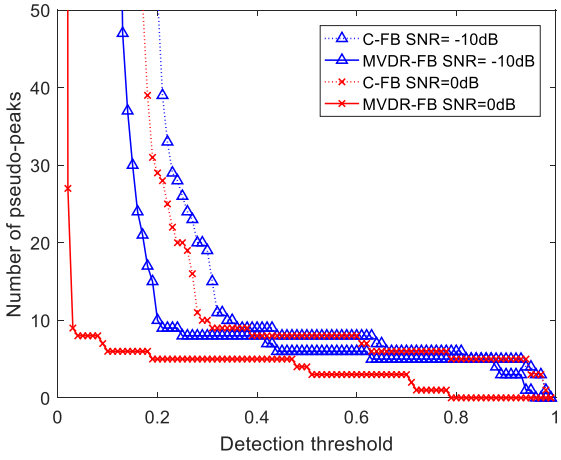

FIGURE 14. The number of pseudo-peaks in terms of the detection threshold.

In the practical application of sonar detection, if the detection threshold γ is set smaller, pseudo-peaks will appear in large numbers and seriously interfere with target detection, but when the γ is set larger, many real targets may be lost; thus, one needs a criterion for choosing an intermediate value of the threshold. Fig. 14 shows that the number of pseudo-peaks was strongly affected by the detection threshold γ. At the beginning, the number of pseudo-peaks changed rapidly, but with the increase of γ, the change gradually slowed down and eventually converged. This convergence shows that the real impact on detection performance and multitarget resolution is caused by a fixed number of pseudo-peaks.

From the simulation in this section, we concluded that the value of γ should be set where the number of pseudo-peaks tends to change slowly or converge. For example, according to Fig. 14, when the C-FB method is used and the SNR is 0 dB or -10 dB, we suggest that the value of γ should be fixed at 0.3 or 0.4. For MVDR-FB, when the SNR is 0 dB or -10 dB, the value of γ should be fixed at 0.1 or 0.2. The lower value of detection threshold needed for MVDR-FB reflects the fact that it generates fewer pseudo-peaks than C-FB.

V. CONCLUSION

In this paper, focused beamformers were used in passive underwater acoustic localization. The pseudo-peak in the focused beamformer spectrum was defined, and the method of its quantity survey was given. The performances of the C-FB and MVDR-FB algorithms were compared based on the number of pseudo-peaks generated. Simulations were performed in a typical underwater acoustic environment, and the localization results were plotted under different conditions, such as different SNRs, distances, frequencies, and detection thresholds. These simulations consistently showed MVDR-FB to be superior to C-FB, producing fewer and

smaller pseudo-peaks. For a modestly high SNR (10 dB), MVDR-FB eliminated pseudo-peaks entirely, unlike C-FB. Its superior performance allowed us to set a lower detection threshold when using MVDR-FB, reflecting a greater sensitivity to weak signals. We also found that the number of pseudo-peaks is affected by this detection threshold, but in a regular manner. As the detection threshold increases, the number of pseudo-peaks tends to change slowly or converge; therefore, we proposed that the detection threshold should be set at this point of changing slowly or convergence. This not only ensures the detection of the target, but also removes unnecessary interference. This proposal for setting detection threshold can be applied to sonar improvement for underwater target detection and identification in the future, whether using the C-FB or the superior MVDR-FB method.

REFERENCES

[1] H. A. Cirpan and E. Cekli, "Deterministic maximum likelihood approach for localization of near-field sources," *AEU-Int. J. Electron. Commun.*, vol. 56, no. 1, pp. 1–10, Nov. 2004.
[2] N. Kabaoğlu, H. A. Çirpan, E. Çekli, and S. Paker, "Deterministic maximum likelihood approach for 3-D near field source localization," *AEU-Int. J. Electron. Commun.*, vol. 57, no. 5, pp. 345–350, Nov. 2004.
[3] J.-J. Jiang, F.-J. Duan, J. Chen, Y.-C. Li, and X.-N. Hua, "Mixed near-field and far-field sources localization using the uniform linear sensor array," *IEEE Sensors J.*, vol. 13, no. 8, pp. 3136–3143, Aug. 2013.
[4] J. Liang and D. Liu, "Passive localization of near-field sources using cumulant," *IEEE Sensors J.*, vol. 9, no. 8, pp. 953–960, Aug. 2009.
[5] J. Liang and D. Liu, "Passive localization of mixed near-field and far-field sources using two-stage MUSIC algorithm," *IEEE Trans. Signal Process.*, vol. 58, no. 1, pp. 108–120, Jan. 2010.
[6] J. Hui, D. Hu, J. Hui, and J. Yin, "Researches on the measurement of distribution image of radiated noise using focused beamforming," *Acta Acust.*, vol. 32, no. 4, pp. 356–361, Apr. 2007.
[7] J. Shi, D.-S. Yang, B.-S. Liu, and H.-Y. Song, "Radiated noise sources near-field location based on MVDR focused beamforming," *J. Dalian Maritime Univ.*, vol. 34, no. 3, pp. 55–58, Aug. 2008.
[8] J. Shi and D.-S. Yang, "Coherent broadband MVDR focused beamforming based on vector sensor array processing," *J. Syst. Simul.*, vol. 22, no. 2, pp. 473–477, Feb. 2010.
[9] L. Kumar and R. M. Hegde, "Near-field acoustic source localization and beamforming in spherical harmonics domain," *IEEE Trans. Signal Process.*, vol. 64, no. 13, pp. 3351–3361, Jul. 2016.
[10] S. D. Somasundaram, N. H. Parsons, P. Li, and R. C. de Lamare, "Reduced-dimension robust capon beamforming using Krylov-subspace techniques," *IEEE Trans. Aerosp. Electron. Syst.*, vol. 51, no. 1, pp. 270–289, Jan. 2015.
[11] D. Salvati, C. Drioli, and G. L. Foresti, "A weighted MVDR beamformer based on SVM learning for sound source localization," *Pattern Recognit. Lett.*, vol. 84, no. 1, pp. 15–21, Dec. 2016.
[12] G. Liu and X. Sun, "Spatial differencing method for mixed far-field and near-field sources localization," *IEEE Signal Process. Lett.*, vol. 21, no. 11, pp. 1331–1335, Nov. 2014.
[13] G. Liu and X. Sun, "Two-stage matrix differencing algorithm for mixed far-field and near-field sources classification and localization," *IEEE Sensors J.*, vol. 14, no. 6, pp. 1957–1965, Jun. 2014.
[14] H. Chen, C.-P. Hou, Q. Wang, L. Huang, and W.-Q. Yan, "Cumulants-based Toeplitz matrices reconstruction method for 2-D coherent doa estimation," *IEEE Sensors J.*, vol. 14, no. 8, pp. 2824–2832, Aug. 2014.
[15] Q. Wu, F. Sun, P. Lan, G. Ding, and X. Zhang, "Two-dimensional direction-of-arrival estimation for co-prime planar arrays: A partial spectral search approach," *IEEE Sensors J.*, vol. 16, no. 14, pp. 5660–5670, Jul. 2016.
[16] K. L. Bell, Y. Ephraim, and H. L. V. Trees, "A Bayesian approach to robust adaptive beamforming," *IEEE Trans. Signal Process.*, vol. 48, no. 2, pp. 386–398, Feb. 2000.
[17] J. Capon, "High-resolution frequency-wavenumber spectrum analysis," *Proc. IEEE*, vol. 57, no. 8, pp. 1408–1418, Aug. 1969.

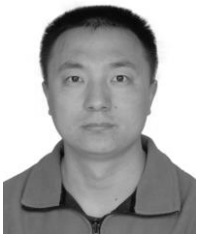

JUN LI (S'17) was born in Yuncheng city, China, in 1981. He received the B.S. degree in SPC Switching Engineering from the Naval University of Engineering, Wuhan, China, in 2003, and the M.S. degree in signal and information processing from Dalian Naval Academy, Dalian, China, in 2008. He is currently pursuing the Ph.D. degree in signal and information processing with the Dalian University of Technology, Dalian, China.

From 2008 to 2009, he was a Teaching Assistant with Dalian Naval Academy, Dalian, China. Since 2010, he has been a Lecturer with the Department of Underwater Weaponry and Chemical Defense. His research interest includes sonar passive localization, underwater acoustic signal processing, and communication.

QIU-HUA LIN (M'10) received the B.S. degree in wireless communication in 1991, the M.S. degree in communications and electronic systems in 1994, and the Ph.D. degree in signal and information processing in 2006, all from Dalian University of Technology, Dalian, China.

She has been with Dalian University of Technology, since 1994. She was a Teaching Assistant from 1994 to 1995, a Lecturer from 1996 to 2001, and an Associate Professor from 2002 to 2006. She was a Visiting Scholar with the University of New Mexico, Albuquerque, NM, USA, in 2006. Since 2007, she has been a Professor with the School of Information and Communication Engineering. Her research interests include array signal processing, biomedical signal processing, image processing, and machine learning.

KAI WANG received the B.S. degree in computer science and technology from Jilin University, Changchun, China, in 2003, and the M.S. degree in computer science and technology from the Beijing University of Posts and Telecommunications, Beijing, China, in 2006.

She has been with Dalian Neusoft Institute of Information, Dalian, China, since 2006. She was a Teaching Assistant from 2006 to 2008 and a Lecturer from 2009 to 2013. Since 2014, she has been an Associate Professor with the Department of Computer Science and Technology. Her research interest includes computer science and technology and underwater acoustic communication and network.

CHUN-YU KANG received the B.S. and M.S. degrees in underwater acoustic electronic engineering from the Naval University of Engineering, Wuhan, China, in 2001 and the Ph.D. degree in combat command from Dalian Naval Academy, Dalian, China, in 2009.

He has been with Dalian Naval Academy, Dalian, China, since 2001. He was a Teaching Assistant from 2001 to 2003 and a Lecturer from 2003 to 2011. Since 2012, he has been an Associate Professor with the Department of Underwater Weaponry and Chemical Defense. His research interest includes underwater acoustic signal processing, sonar systems and passive localization.